Resonant frequencies of a radial field piezoelectric diaphragm

***Xingxu Zhang[1,2], Xiaobiao Shan[1], †Tao Xie[1] and †Jianmin Miao[2].**

[1]State Key Laboratory of Robotics and System, Harbin Institute of Technology, Harbin 150001, China;
[2]School of Mechanical and Aerospace Engineering, Nanyang Technological University, 639798, Singapore.
*Presenting author: 16B908021@stu.hit.edu.cn

†Corresponding author: xietao@hit.edu.cn; mjmmiao@ntu.edu.sg.

Abstract

This paper presents a circular piezoelectric diaphragm which has a radial polarization distribution by using inter-circulating electrodes. An equation for calculating the resonant frequency of the radial field piezoelectric diaphragm is obtained based on the thin plate elastic theory combined with the Rayleigh-Ritz method. The finite element analysis (FEA) was used to predict the resonant frequency of the radial field piezoelectric diaphragm. To verify the theoretical analysis, the impedance characteristic of the radial field piezoelectric diaphragm was measured using an experimental method. The results obtained from theoretical analysis were in good agreement with those from the FEA and experimental results. The effect of geometrical changes to the first resonance frequency of the diaphragm is also described. The calculated results were found to be in good agreement with the FEA results. The results indicate that the resonant frequency of the radial field piezoelectric diaphragm decreases from 16.43 kHz to 11.92 kHz when the diameter increases from 9.2 mm to 10.8 mm.

Keywords: Radial field diaphragm, Piezoelectric transducer, Resonant frequency, Rayleigh-Ritz method.

Introduction

Circular piezoelectric diaphragms are commonly employed for the purpose of sensing and actuating, such as electroacoustic devices [1], micromotors [2,3], microfluidic pumps [4] and so on. They are also widely used as energy harvesters [5,6]. Cui et al. [7] proposed a multi-layer piezoelectric structure working as an actuator for valveless pumps. They established an analytical model and verified it by finite element analysis. Kim et al. [8] analyzed a clamped circular piezoelectric plate with different electrode patterns to enhance the power generation of energy harvesters. Papila et al. [9] addressed the design of a clamped circular piezoelectric composite diaphragm with oppositely polarized piezoceramic patches. Smyth et al. [10] modeled a micromachined piezoelectric ultrasonic transducer with circular and ring electrodes. Piezoelectric elements in these transducers work in d_{31} mode. However, because the d_{33} parameter is usually two times that of the d_{31} parameter, the PZT elements which work in d_{33} mode are more efficient when the transducers have the similar geometrical structure under the same pressure [11].

For the circular diaphragm structure, it is generally difficult to do in-plane poling due to the much bigger scale in the radial direction. Bryant et al. [12,13] designed equivalent d_{33} mode piezoelectric diaphragms poled by interdigitated ring electrodes or inter-circulating electrodes. Hong et al. [14-16] designed micromachined radial field piezoelectric diaphragms with interdigitated ring electrodes. Wang et al. [17] proposed radial field piezoelectric diaphragms with interdigitated ring electrodes using bulk PZT materials. Shen et al. [18,19] designed piezoelectric diaphragms with spiral electrodes to perform in-plane poling. For piezoelectric transducers, the fundamental resonance is generally the most important one [19]. However, most of the studies utilized finite element analysis and experiments to characterize the radial field piezoelectric diaphragm. Theoretical analysis of calculating the fundamental resonant frequency of the radial field piezoelectric diaphragms has been rarely reported.

Hence, in this paper, an equation for calculating the fundamental resonant frequency of the radial field piezoelectric diaphragms was established. Finite element analysis was used to analyze the vibration mode. Experiments were conducted to verify the theoretical analysis. Besides, the influence of geometrical parameters of the diaphragms was also discussed.

Theoretical Analysis

Figure 1 shows a schematic diagram of a piezoelectric diaphragm. Figure 2 shows a schematic diagram of the electrode pattern on the surfaces of PZT with polarization orientation. A circular piezoelectric wafer was bonded with a polymethyl methacrylate (PMMA) substrate which had a through hole. There are inter-circulating electrodes on the surfaces of the piezoelectric wafer. When a poling electric field is applied to the electrodes, the result is a radial polarization distribution. Hence, a radial field piezoelectric diaphragm is obtained. The diaphragm has a diameter of d_1 and thickness of h. Its diameter is much larger than its thickness. Because the thickness of the electrodes is as small as 400 nm, the mass and stiffness of the electrodes have little influence on the system dynamic properties and they will be ignored during the theoretical analysis.

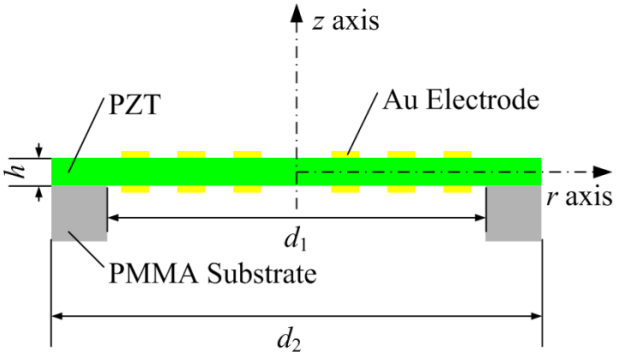

Figure 1. Schematic diagram of a piezoelectric diaphragm

Here, a cylindrical coordinate system was adopted in order to conveniently conduct theoretical analysis due to the circular diaphragm structure. When an electric field is applied to the electrodes, the induced strain in the piezoelectric diaphragm will lead to a flexural deformation. The deformation is much smaller than its thickness. According to the Kirchholf-Love thin plate elastic theory, the strains and stresses in some directions in the

piezoelectric element are given as

$$S_z = S_{zr} = S_{\theta z} = S_{r\theta} = 0 \tag{1}$$

$$T_z = 0 \tag{2}$$

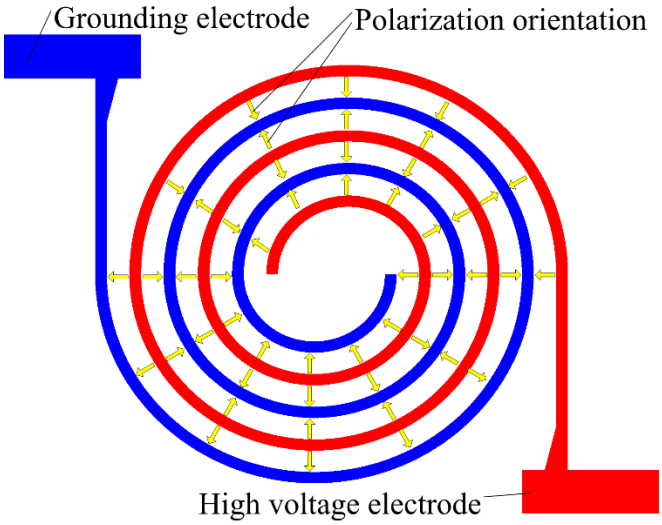

Figure 2. Electrode pattern on the PZT with polarization orientation

Based on the d-type piezoelectric equations, the constitutive equations are obtained as [20,21]

$$S_\theta = s_{11}^E T_\theta + s_{13}^E T_r + d_{31} D_r \tag{3a}$$

$$S_r = s_{13}^E T_\theta + s_{33}^E T_r + d_{33} D_r \tag{3b}$$

$$D_r = d_{31} T_\theta + d_{33} T_r + \varepsilon_{33}^T E_r \tag{3c}$$

where S_θ and S_r are the circumferential and radial strains of the piezoelectric element, respectively; T_θ and T_r are the circumferential and radial stresses of the piezoelectric element, respectively; D_r and E_r are the electric displacement and electric field, respectively; s_{11}^E, s_{13}^E, and s_{33}^E are the compliance coefficients at constant electric field; d_{31} and d_{33} are the piezoelectric coefficients; ε_{33}^T is the permittivity of the piezoelectric element at constant stress. According to Eq. (3), the stresses in the piezoelectric element can be described as

$$T_\theta = \lambda_1 S_\theta + \lambda_2 S_r + \lambda_3 D_r \tag{4a}$$

$$T_r = \lambda_2 S_\theta + \lambda_4 S_r + \lambda_5 D_r \tag{4b}$$

$$E_r = \lambda_6 S_\theta + \lambda_7 S_r + \lambda_8 D_r \tag{4c}$$

where λ_1, λ_2, λ_3, λ_4, λ_5, λ_6, λ_7, and λ_8 are a series of constants. They are expressed as follows

$$\lambda_1 = \frac{s_{33}^E}{s_{11}^E s_{33}^E - s_{13}^E s_{13}^E} \tag{5a}$$

$$\lambda_2 = \frac{-s_{13}^E}{s_{11}^E s_{33}^E - s_{13}^E s_{13}^E} \tag{5b}$$

$$\lambda_3 = \frac{s_{13}^E d_{33} - s_{33}^E d_{31}}{s_{11}^E s_{33}^E - s_{13}^E s_{13}^E} \tag{5c}$$

$$\lambda_4 = \frac{s_{11}^E}{s_{11}^E s_{33}^E - s_{13}^E s_{13}^E} \tag{5d}$$

$$\lambda_5 = \frac{s_{13}^E d_{31} - s_{11}^E d_{33}}{s_{11}^E s_{33}^E - s_{13}^E s_{13}^E} \tag{5e}$$

$$\lambda_6 = \frac{-d_{31}\lambda_1 - d_{33}\lambda_2}{\varepsilon_{33}^T} \tag{5f}$$

$$\lambda_7 = \frac{-d_{31}\lambda_2 - d_{33}\lambda_4}{\varepsilon_{33}^T} \tag{5g}$$

$$\lambda_8 = \frac{1-d_{31}\lambda_3 - d_{33}\lambda_5}{\varepsilon_{33}^T} \tag{5h}$$

There is no free charge on the surfaces of the piezoelectric diaphragm, hence the charge equation of electrostatics is [22]

$$\frac{1}{r}\frac{\partial}{\partial r}(rD_r) = 0 \tag{6}$$

Based on the thermodynamic equilibrium principle, D_{p}, which is the strain energy density of an infinitesimal volume element in piezoelectric material, is written as

$$D_{\mathrm{p}} = \frac{1}{2}T_r S_r + \frac{1}{2}T_\theta S_\theta \tag{7}$$

By substituting Eq. (4) into Eq. (7), the D_{p} is obtained as

$$D_{\mathrm{p}} = \frac{1}{2}\lambda_1 S_\theta^2 + \frac{1}{2}\lambda_4 S_r^2 + \lambda_2 S_\theta S_r + \frac{1}{2}(\lambda_3 S_\theta + \lambda_5 S_r)D_r \tag{8}$$

The strains in the diaphragm has the relationship with the curvature of the mid-plane as

$$S_r = z\mu_r \tag{9a}$$

$$S_\theta = z\mu_\theta \tag{9b}$$

where z is the distance from the natural surface; μ_{r} and μ_θ are the curvatures of mid-plane, and they are defined as [23]

$$\mu_r = -\frac{\partial^2 w}{\partial r^2} \tag{10a}$$

$$\mu_\theta = -\frac{1}{r}\frac{\partial w}{\partial r} \tag{10b}$$

where w is the displacement in the z-axis direction. The diaphragm is in the status of simple harmonic vibration

$$w = w_z \sin(\omega t) \tag{11}$$

where w_z is the vibration mode displacement function, t is time, ω is angular frequency.
By substitution of Eq. (9) into Eq. (8) and integration in the thickness direction, the unit area of the strain energy in the piezoelectric element is given by

$$u_p = \int_z D_{\mathrm{p}} \mathrm{d}z = \frac{h^3}{24}\left(\frac{1}{2}\lambda_1\mu_\theta^2 + \lambda_2\mu_\theta\mu_r + \frac{1}{2}\lambda_4\mu_r^2\right) \tag{12}$$

The total strain energy of the piezoelectric diaphragm can be obtained by an area integration

$$U = \iint_s u_p \mathrm{d}s = \frac{\pi h^3}{12}\int_0^{d_1/2}\left(\frac{1}{2}\lambda_1\mu_\theta^2 + \lambda_2\mu_\theta\mu_r + \frac{1}{2}\lambda_4\mu_r^2\right)r\mathrm{d}r \tag{13}$$

The kinetic energy of the radial field piezoelectric diaphragm can be denoted as

$$T = \frac{1}{2}\iint_s \left(\frac{\partial w}{\partial t}\right)^2 \mathrm{d}s = \rho\pi h\int_0^{d_1/2}\left(\frac{\partial w}{\partial t}\right)^2 r\mathrm{d}r \tag{14}$$

where ρ is the density of the PZT.
The electric energy of the radial field piezoelectric diaphragm can be calculated as

$$U^{\mathrm{E}} = \iiint_V E_r D_r \mathrm{d}V = \int_0^{2\pi}\mathrm{d}\theta\int_0^{d_1/2}\mathrm{d}r\int_{-h/2}^{h/2} E_r D_r r\mathrm{d}z \tag{15}$$

Based on the Rayleigh-Ritz method and the symmetrical structure, the functional analysis of the radial field piezoelectric diaphragm can be given as [23]

$$L = U_{\max} - T_{\max} - U_{\max}^{\mathrm{E}} \tag{16}$$

where $U_{\max}$ is the maximal strain energy, $T_{\max}$ is the maximal kinetic energy, $U_{\max}^{\mathrm{E}}$ is the maximal electric energy, respectively, of the radial field piezoelectric diaphragm.
By substituting Eqs. (10), (13), (14), (15) into Eq. (16), the functional analysis is obtained as

$$\begin{aligned} L = {} & \frac{\pi h^3}{12}\int_0^{d_1/2}\left[\frac{1}{2}\lambda_1\left(-\frac{1}{r}\frac{\partial w_z}{\partial r}\right)^2 + \lambda_2\frac{\partial w_z^2}{\partial r^2}\frac{1}{r}\frac{\partial w_z}{\partial r} + \frac{1}{2}\lambda_4\left(-\frac{\partial w_z^2}{\partial r^2}\right)^2\right]r\mathrm{d}r \\ & -\rho\pi h\omega^2\int_0^{d_1/2} w_z^2 r\mathrm{d}r - 2\pi h\int_0^{d_1/2}\lambda_8 D_r^2 r\mathrm{d}r \end{aligned} \tag{17}$$

When the diaphragm has a clamped boundary, the boundary condition can be written as

$$w_z = 0 \tag{18a}$$

$$\frac{\mathrm{d}w_z}{\mathrm{d}r} = 0 \tag{18b}$$

where $r = d_1/2$.

The approximate vibration mode displacement function can be written as [8]

$$w_z = A(\frac{1}{4}d_1^2 - r^2)^2 \tag{19}$$

By substituting Eq. (19) into Eq. (17), then solve the equation

$$\frac{\mathrm{d}L}{\mathrm{d}A} = 0 \tag{20}$$

Finally, the fundamental resonant angular frequency ω will be obtained.

Finite Element Analysis

Finite element method was also employed here to analyze the influence of geometrical parameters on the fundamental resonant frequency. The element SOLID 226 was selected to conduct the modal analysis. A circular diaphragm model with inter-circulating electrodes was established and the edge of the circular diaphragm was set as clamped boundary. The radial polarization distribution was released by rotating the local element coordinate systems after comparing the poling electric field strength with the coercive field strength. The PZT5A parameters are given below as: s_{11}^{E}=15.4×10^{-12} m^2/N, s_{12}^{E}=-4.8×10^{-12} m^2/N, s_{13}^{E}=-8.4×10^{-12} m^2/N, s_{33}^{E}=15.4×10^{-12} m^2/N, s_{44}^{E}=47.8×10^{-12} m^2/N, s_{66}^{E}=40.4×10^{-12} m^2/N, d_{31}=-191×10^{-12} C/N, d_{33}=430×10^{-12} C/N, d_{15}=590×10^{-12} C/N, ε_{11}=1780ε_0, ε_{33}=1950ε_0, ε_0=8.854×10^{-12} F/m, where s_{ij}^{E}, d_{ij} and ε_{ij} are the elastic compliance, piezoelectric and permittivity constants, respectively, where i, j (i, j = 1, 2, 3, 4, 5, 6) denote tensor notation. Diaphragm models with different diameters and thicknesses were built and their fundamental resonant frequencies were calculated.

Figure 3 shows some modal analysis simulation results. Figure 3a shows the fundamental resonant vibration mode of the piezoelectric diaphragm with a diameter of 10 mm and thickness of 0.3 mm. Figure 3b shows the fundamental resonant vibration mode of the piezoelectric diaphragm with a diameter of 10 mm and thickness of 0.127 mm. From Figure 3, one can know that the fundamental resonant frequency will increase with the increase of thickness. More detailed results will be discussed in next section.

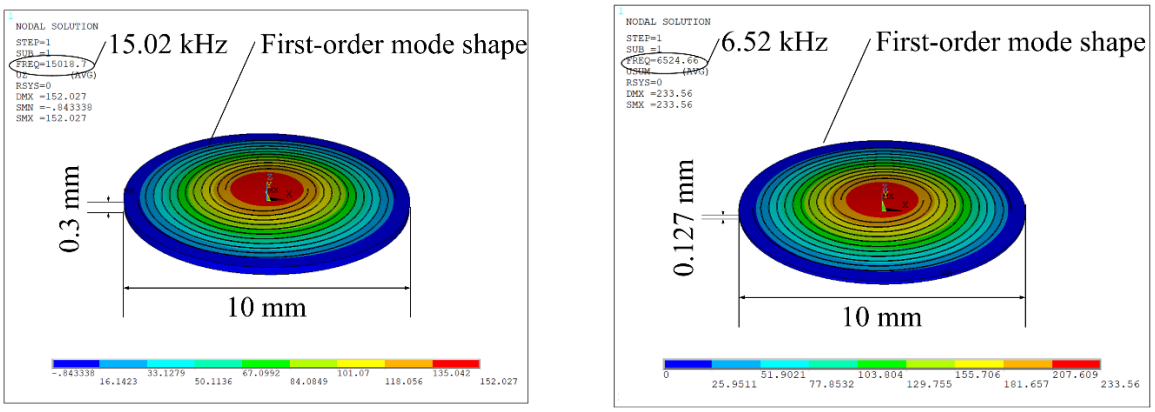

(**a**) (**b**)

Figure 3. Modal analysis simulation results: (a) Fundamental resonant frequency of the piezoelectric diaphragm with diameter of 10 mm and thickness of 0.3 mm: f_1 = 15.02 kHz, (b) Fundamental resonant frequency of the piezoelectric diaphragm with diameter of 10 mm and thickness of 0.127 mm: f_1 = 6.52 kHz.

Experiments and Results

Inter-circulating electrodes on the surfaces of PZT were fabricated using micro-fabrication technology in a clean room. Figure 4 shows a schematic diagram of the fabrication procedure. Photolithography, magnetron sputtering and lift-off process were conducted. More details were described in [24].

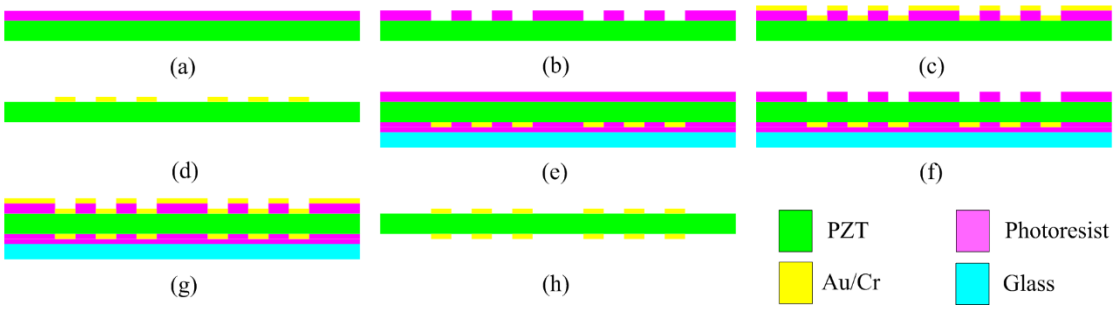

Figure 4. Schematics of the device fabrication process. (a) Photoresist spin coating; (b) Photolithography; (c) Magnetron sputtering; (d) Lift off process; (e) Backside photoresist spin coating; (f) Backside alignment photolithography; (g) Backside magnetron sputtering; (h) Lift off process

Then the PZT wafer was bonded with a PMMA substrate. Wire connection and poling process were conducted. Hence a radial field piezoelectric diaphragm was obtained. The diaphragm has a diameter of 10 mm and thickness of 0.3 mm. An impedance analyzer (Agilent 4294A, Agilent Technologies Inc., Santa Clara, CA, USA) was utilized to measure the resonant frequency of the diaphragm.

Figure 5 shows a photograph of the impedance and phase spectrum testing. Figure 6 shows the impedance and phase spectrum of the diaphragm. The frequencies of the theoretical analysis, finite element analysis and experiment results are 13.91 kHz, 15.02 kHz and 14.36 kHz, respectively. The results of theoretical analysis were in good agreement with those of

finite element analysis and experiment results.

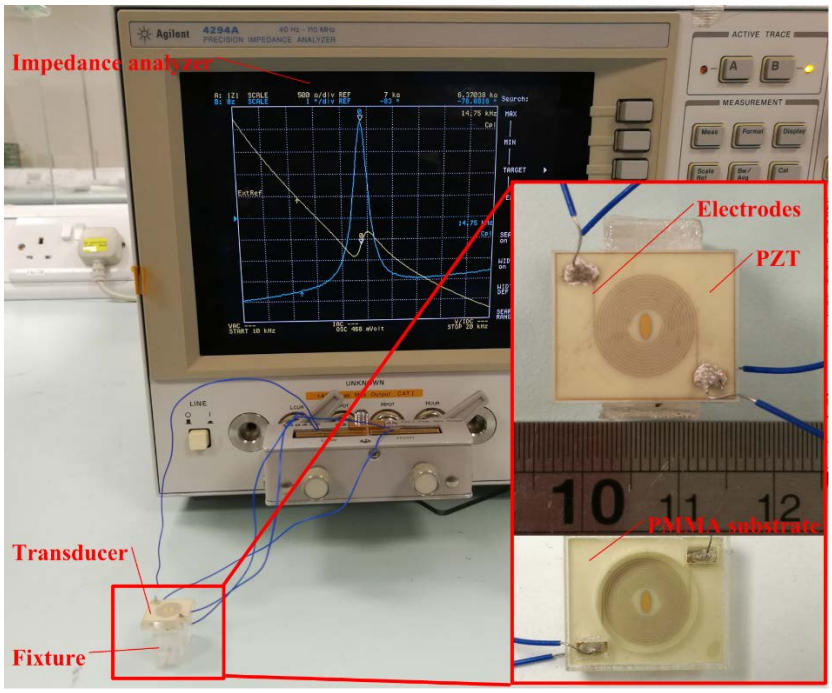

Figure 5. Impedance and phase spectrum testing

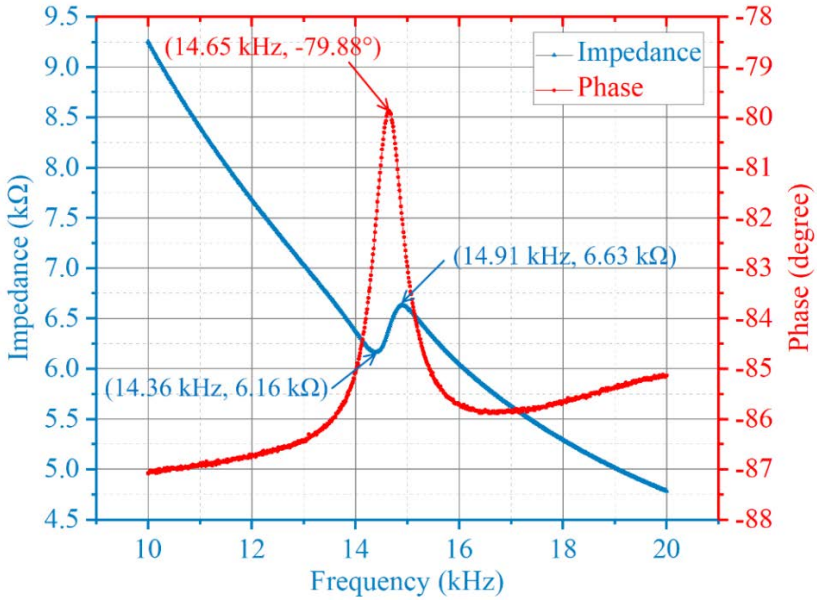

Figure 6. Impedance and phase spectrum of the diaphragm

As mentioned in previous sections, the diameter of the piezoelectric diaphragm has a profound effect on the fundamental resonant frequency. Figure 7 shows the results obtained from the theoretical analysis and finite element analysis with different diameters. From Figure 7, one can know that the theoretical results are in good agreement with the finite element analysis results. The fundamental resonant frequency will decrease from 16.43 kHz to 11.92 kHz when the diameter increases from 9.2 mm to 10.8 mm.

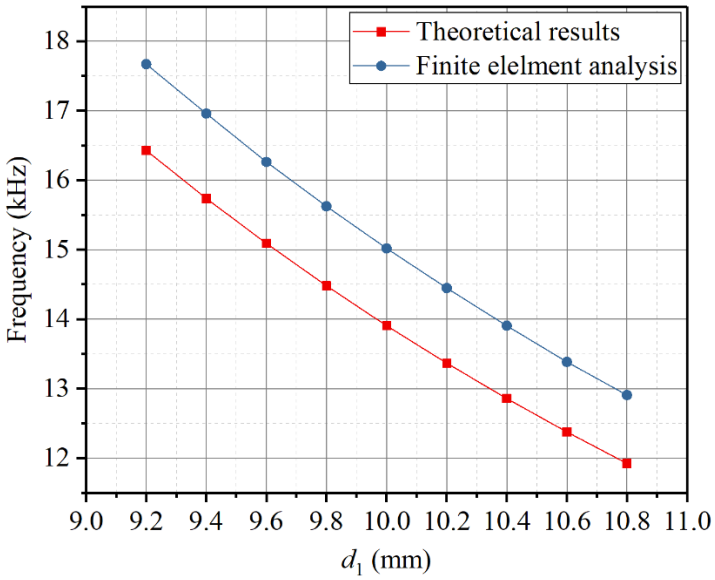

Figure 7. Frequency-diameter curves of the piezoelectric diaphragm

Conclusion

Based on the Kirchholf-Love thin plate elastic theory and piezoelectric equations combined with the Rayleigh-Ritz method, an equation for calculating the fundamental resonant frequency of a radial field piezoelectric diaphragm was obtained. Finite element analysis (FEA) was conducted to calculate the resonant vibration mode. Prototype was fabricated by microfabrication technology in a clean room and its impedance spectrum was examined by an impedance analyzer. The theoretical analysis results were in good agreement with the FEA and experimental results. The effect of geometrical parameters on the fundamental resonant frequency was also analyzed. The results showed that the fundamental resonant frequency of the radial field piezoelectric diaphragm decreases from 16.43 kHz to 11.92 kHz when the diameter increases from 9.2 mm to 10.8 mm.

Acknowledgements

This work is supported by the National Natural Science Foundation of China (Grant No. 51677043) and the China Scholarship Council (Grant No. 201706120130).

References

1. Prasad, S.A.; Gallas, Q.; Horowitz, S.B.; Homeijer, B.D.; Sankar, B.V.; Cattafesta, L.N.; Sheplak, M. Analytical electroacoustic model of a piezoelectric composite circular plate. *AIAA journal* **2006**, *44*, 2311-2318.
2. Deshpande, M.; Saggere, L. An analytical model and working equations for static deflections of a circular multi-layered diaphragm-type piezoelectric actuator. *Sensors and Actuators A: Physical* **2007**, *136*, 673-689.
3. Wright, R.; Mo, C.; Clark, W.W. Effect of electrode pattern on the performance of unimorph piezoelectric diaphragm actuators. In Proceedings of Smart Structures and Materials 2005: Smart Structures and Integrated Systems; pp. 42-50.
4. He, X.; Xu, W.; Lin, N.; Uzoejinwa, B.; Deng, Z. Dynamics modeling and vibration analysis of a piezoelectric diaphragm applied in valveless micropump. *Journal of Sound and Vibration* **2017**, *405*, 133-143.

5. Yang, Y.; Wang, S.; Stein, P.; Xu, B.-X.; Yang, T. Vibration-based energy harvesting with a clamped piezoelectric circular diaphragm: analysis and identification of optimal structural parameters. *Smart Materials and Structures* **2017**, *26*, 045011.
6. Mo, C.; Radziemski, L.J.; Clark, W.W. Analysis of piezoelectric circular diaphragm energy harvesters for use in a pressure fluctuating system. *Smart Materials and Structures* **2010**, *19*, 025016.
7. Cui, Q.; Liu, C.; Zha, X.F. Modeling and numerical analysis of a circular piezoelectric actuator for valveless micropumps. *Journal of intelligent material systems and structures* **2008**, *19*, 1195-1205.
8. Kim, S.; Clark, W.W.; Wang, Q.-M. Piezoelectric energy harvesting with a clamped circular plate: analysis. *Journal of intelligent material systems and structures* **2005**, *16*, 847-854.
9. Papila, M.; Sheplak, M.; Cattafesta III, L.N. Optimization of clamped circular piezoelectric composite actuators. *Sensors and Actuators A: Physical* **2008**, *147*, 310-323.
10. Smyth, K.; Bathurst, S.; Sammoura, F.; Kim, S.-G. Analytic solution for N-electrode actuated piezoelectric disk with application to piezoelectric micromachined ultrasonic transducers. *IEEE transactions on ultrasonics, ferroelectrics, and frequency control* **2013**, *60*, 1756-1767.
11. Shen, Z.; Liu, S.; Miao, J.; Woh, L.S.; Wang, Z. Spiral electrode d33 mode piezoelectric diaphragm combined with proof mass as energy harvester. *Journal of Micromechanics and Microengineering* **2015**, *25*, 035004.
12. Bryant, R.G.; Effinger, R.T.; Aranda, I.; Copeland, B.M.; Covington, E.W. Active piezoelectric diaphragms. In Proceedings of Smart Structures and Materials 2002: Active Materials: Behavior and Mechanics; pp. 303-315.
13. Bryant, R.G.; Effinger Iv, R.T.; Aranda Jr, I.; Copeland Jr, B.M.; Covington Iii, E.W.; Hogge, J.M. Radial field piezoelectric diaphragms. *Journal of intelligent material systems and structures* **2004**, *15*, 527-538.
14. Hong, E.; Krishnaswamy, S.; Freidhoff, C.; Trolier-McKinstry, S. Micromachined piezoelectric diaphragms actuated by ring shaped interdigitated transducer electrodes. *Sensors and Actuators A: Physical* **2005**, *119*, 521-527.
15. Hong, E.; Trolier-McKinstry, S.; Smith, R.; Krishnaswamy, S.V.; Freidhoff, C.B. Vibration of micromachined circular piezoelectric diaphragms. *IEEE transactions on ultrasonics, ferroelectrics, and frequency control* **2006**, *53*, 697-706.
16. Hong, E.; Trolier-McKinstry, S.; Smith, R.L.; Krishnaswamy, S.V.; Freidhoff, C.B. Design of MEMS PZT circular diaphragm actuators to generate large deflections. *Journal of Microelectromechanical systems* **2006**, *15*, 832-839.
17. Wang, Z.; Miao, J.; Tan, C.W.; Xu, T. Fabrication of piezoelectric MEMS devices-from thin film to bulk PZT wafer. *Journal of electroceramics* **2010**, *24*, 25-32.
18. Shen, Z.; Olfatnia, M.; Miao, J.; Wang, Z. Displacement and resonance behaviors of a piezoelectric diaphragm driven by a double-sided spiral electrode. *Smart materials and structures* **2012**, *21*, 055001.
19. Shen, Z.; Lu, J.; Tan, C.W.; Miao, J.; Wang, Z. d33 mode piezoelectric diaphragm based acoustic transducer with high sensitivity. *Sensors and Actuators A: Physical* **2013**, *189*, 93-99.
20. Lin, S.; Fu, Z.; Zhang, X.; Wang, Y.; Hu, J. Radially sandwiched cylindrical piezoelectric transducer. *Smart Materials and Structures* **2012**, *22*, 015005.
21. Salowitz, N.P.; Kim, S.-J.; Kopsaftopoulos, F.; Li, Y.-H.; Chang, F.-K. Design and analysis of radially polarized screen-printed piezoelectric transducers. *Journal of Intelligent Material Systems and Structures* **2017**, *28*, 934-946.
22. Chen, W.; Lu, C.; Yang, J.; Wang, J. A circular cylindrical, radially polarized ceramic shell piezoelectric transformer. *IEEE transactions on ultrasonics, ferroelectrics, and frequency control* **2009**, *56*, 1238-1245.
23. Yuan, J.-b.; Xie, T.; Shan, X.-b.; Chen, W.-s. Resonant frequencies of a piezoelectric drum transducer. *Journal of Zhejiang University-SCIENCE A* **2009**, *10*, 1313-1319.
24. Zhang, X.; Shan, X.; Shen, Z.; Xie, T.; Miao, J. A New Self-Powered Sensor Using the Radial Field Piezoelectric Diaphragm in d33 Mode for Detecting Underwater Disturbances. *Sensors* **2019**, *19*, 962.